

Supporting information:

**The $N(^4S) + O_2(X^3\Sigma_g^-) \leftrightarrow O(^3P) + NO(X^2\Pi)$ Reaction: Thermal and Vibrational
Relaxation Rates for the $^2A'$, $^4A'$ and $^2A''$ States**

Juan Carlos San Vicente Veliz,¹ Debasish Koner,¹ Max Schwilk,¹ Raymond J. Bemish,²
and Markus Meuwly¹

¹*Department of Chemistry, University of Basel, Klingelbergstrasse 80,
CH-4056 Basel, Switzerland*

²*Air Force Research Laboratory, Space Vehicles Directorate, Kirtland AFB,
New Mexico 87117, USA*

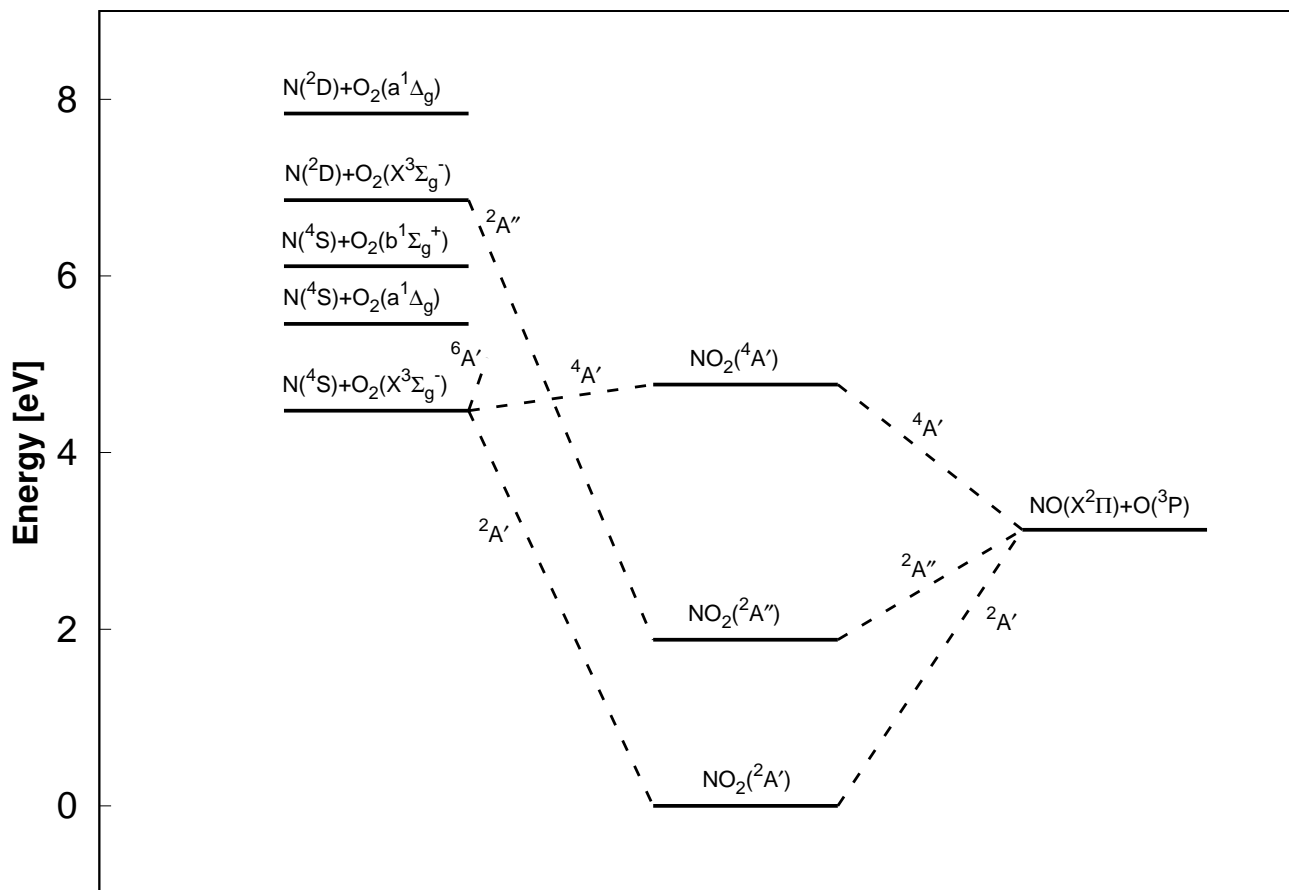


FIG. S1. Correlation plot for the NO₂ states (in *C_S* symmetry) investigated in the present work (middle) and their connection with the atom+diatom states. Only the $^2A'$ and $^2A''$ states have attractive wells with respect to dissociation into atom+diatom states. One of the sextet states discussed in the manuscript is also indicated.

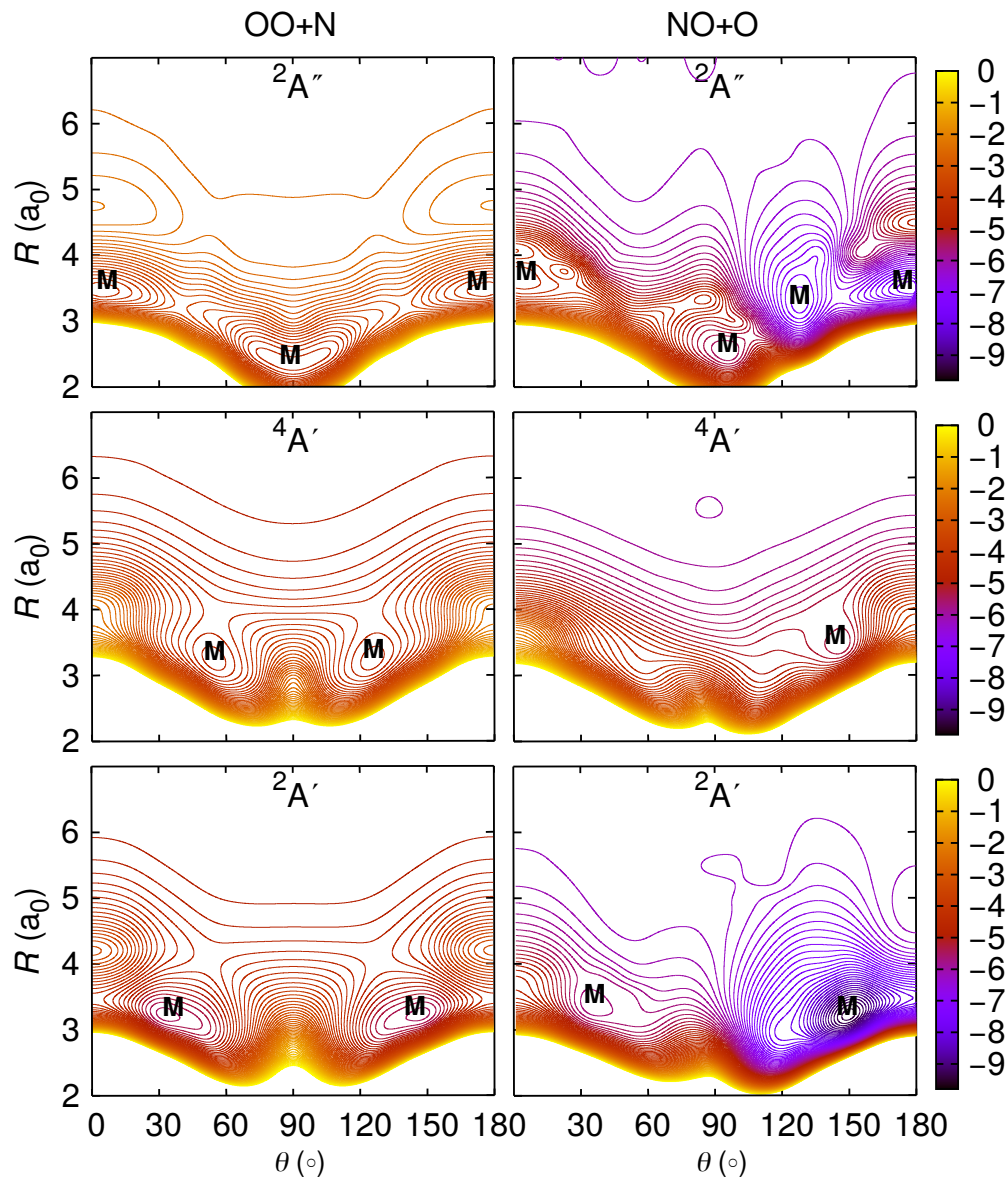


FIG. S2. Two-dimensional cuts through the 3-d PES for the OO+N (left) and the NO+O (right) channels. The OO and NO diatomics are at their equilibrium bond lengths of the respective states, see text. The three states are $^2A''$, $^4A'$, and $^2A'$ from bottom to top. Contour increments of 0.1 eV. The zero of energy is for dissociation into atomic fragments. “M” labels the minima described in the text.

REFERENCES

- ¹G. Henkelman, B. Uberuaga, and H. Jonsson, *J. Chem. Phys.* **113**, 9901 (2000).
- ²E. L. Kolsbjerg, M. N. Groves, and B. Hammer, *J. Chem. Phys.* **145**, 094107 (2016).

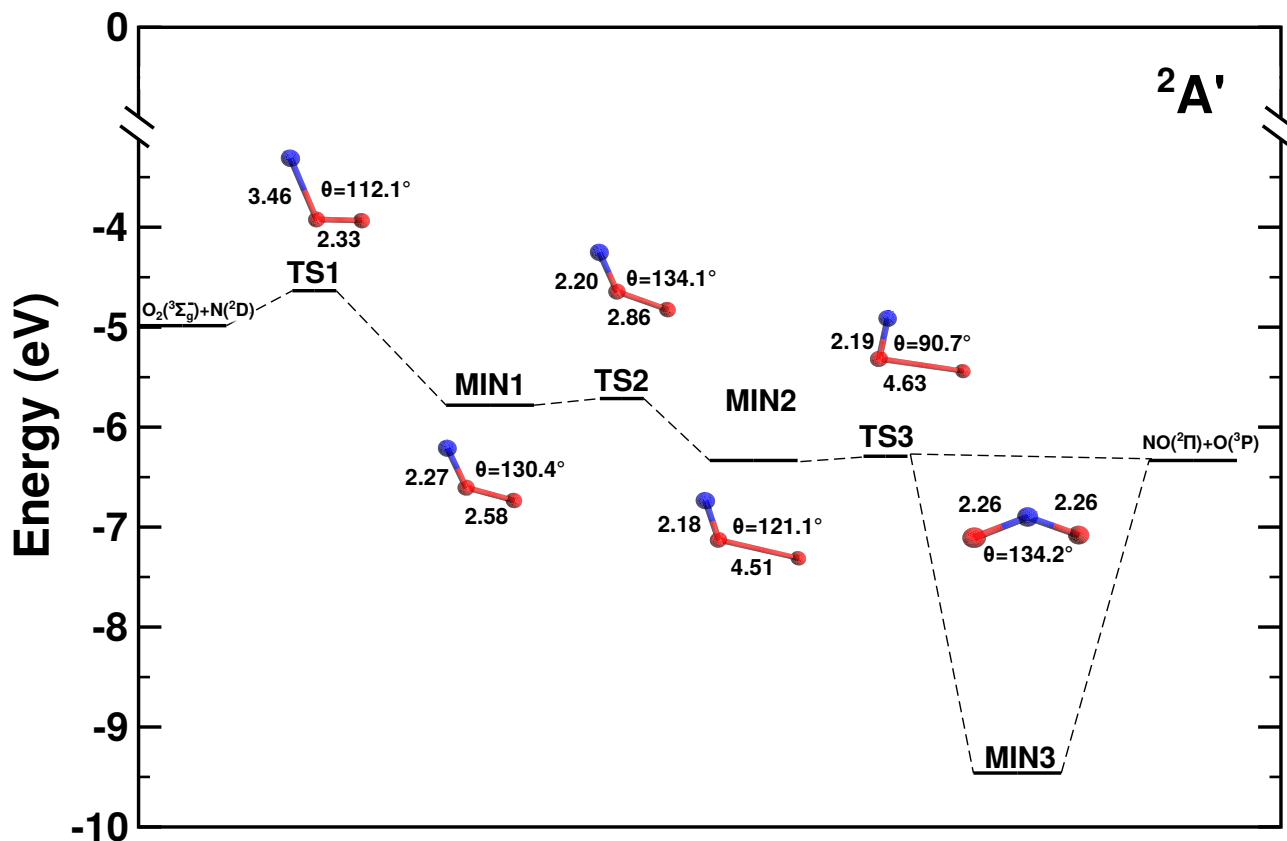


FIG. S3. The minima (MIN_i) and transition states (TS_i) for the $2A'$ state as found from minimization and the nudged elastic band calculations.^{1,2} The geometrical parameters are also given (bond distances in a_0).

³R. Sayós, C. Oliva, and M. González, J. Chem. Phys. **117**, 670 (2002).

⁴P. J. S. B. Caridade, J. Li, V. C. Mota, and A. J. C. Varandas, J. Phys. Chem. A **122**, 5299 (2018).

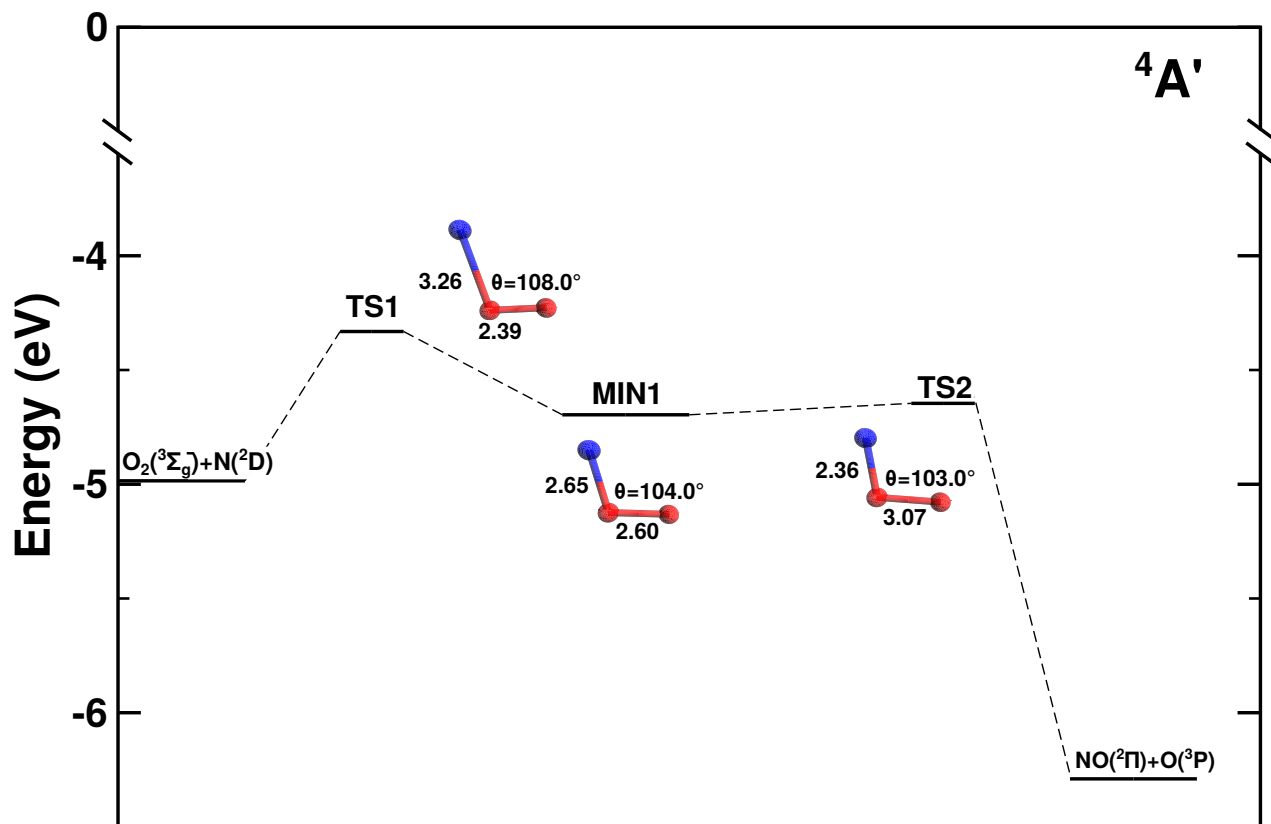


FIG. S4. The minima (MIN_i) and transition states (TS_i) for the $4A'$ state as found from minimization and the nudged elastic band calculations. The geometrical parameters are also given (bond distances in a_0).

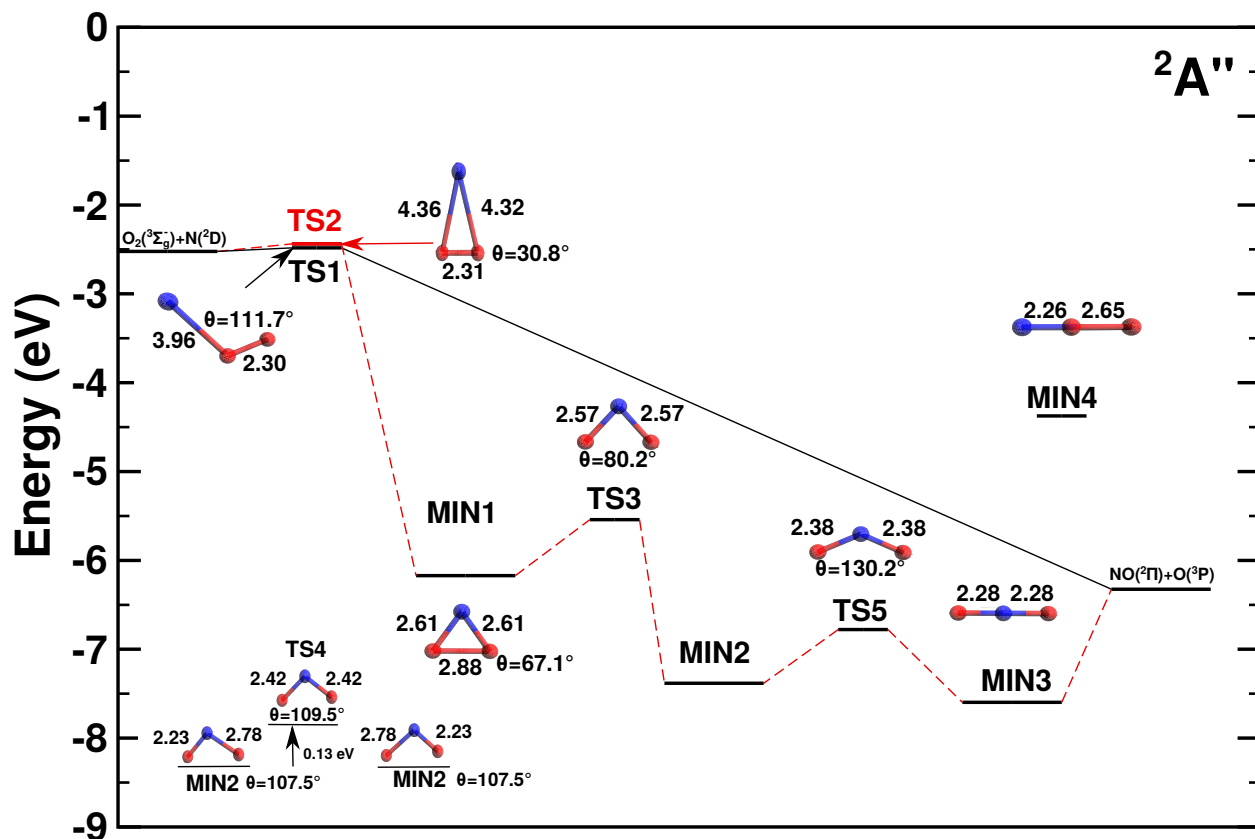


FIG. S5. The minima (MIN_i) and transition states (TS_i) for the $2A''$ state as found from minimization and the nudged elastic band calculations.¹ The geometrical parameters are also given (bond distances in a_0).

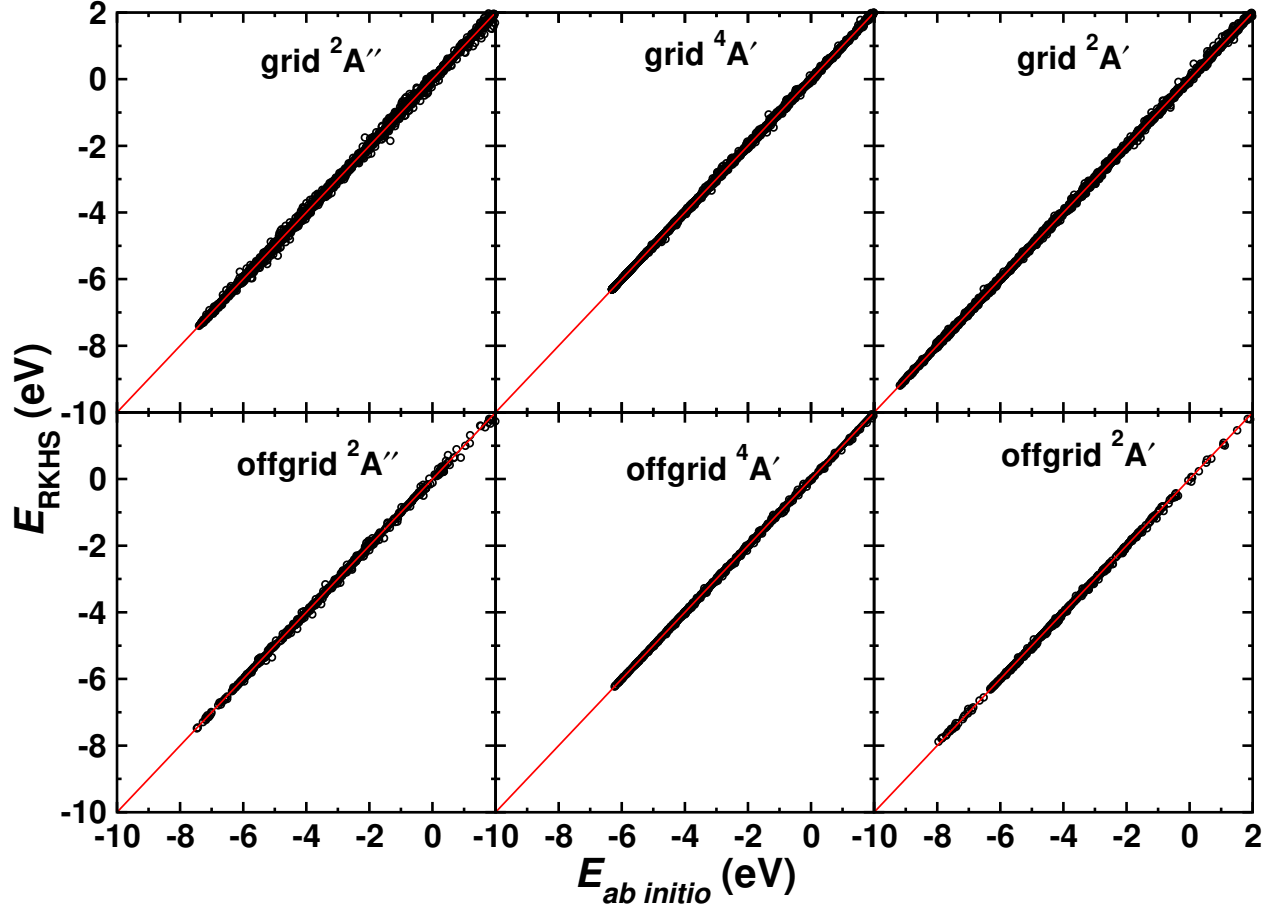
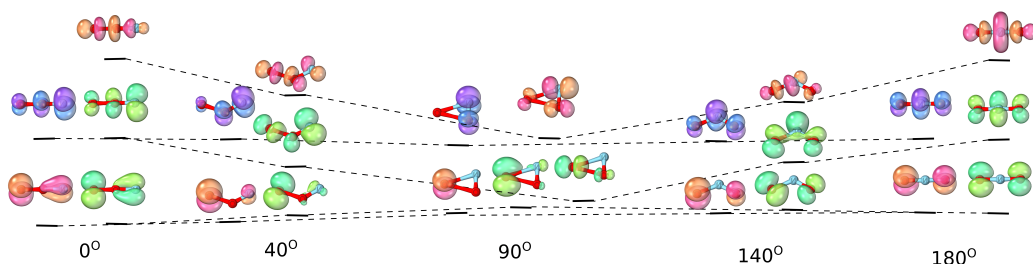


FIG. S6. Correlation between MRCI/aug-cc-PVTZ ($E_{ab\ initio}$) and RKHS energies up to a values of 2 eV for 7435 ($^2A'$), 6869 ($^4A'$) and 7275 ($^2A''$) grid points and 537, 533 and 596 offgrid points for the $^2A'$, $^4A'$ and $^2A''$ surfaces, respectively. The zero of energy is the O+O+N dissociation limit. The R^2 value for the grid points are (0.99984, 0.99989, 0.99965) and for off-grid points (0.99959, 0.99966, 0.99922) for the ($^2A'$, $^4A'$, $^2A''$) surfaces, respectively. The corresponding root mean squared errors (RMSE) for the $^2A'$, $^4A'$ and $^2A''$ surfaces are (0.65, 0.49, 0.99) kcal/mol (0.028, 0.022, 0.043) eV for the grid points and (0.86, 0.76, 1.31) kcal/mol (0.038, 0.033, 0.057) eV for offgrid points.

Natural orbitals with varying occupation number



Dominant configurations of the symmetries

$2^2A'$	A — ↑ ↑ ↔ ↑ — ↑ ↑ ↑ ↑ ↑ 0°/180° 90°	B ↑ ↑ ↑ ↔ ↑ ↑ ↑ ↑ ↑ ↑ ↑ 0°/180° 90°	C — ↑ ↑ ↔ ↑ — ↑ ↑ ↑ ↑ ↑ 0°/180° 90°	D ↑* ↑* ↑* ↔ — — ↑* ↑* ↑* ↑* ↑* 0°/180° 90°	E — ↑* ↑* ↔ — — ↑* ↑* ↑* ↑* ↑* 0°/180° 90°	
$2^2A''$	A — ↑ ↑ ↔ ↑ — ↑ ↑ ↑ ↑ ↑ 0°/180° 90°	B — ↑ ↑ ↔ ↑ — ↑ ↑ ↑ ↑ ↑ 0°/180° 90°	C — ↑ ↑ ↔ — — ↑ ↑ ↑ ↑ ↑ 0°/180° 90°	D — ↑* ↑* ↔ — — ↑* ↑* ↑* ↑* ↑* 0°/180° 90°	E ↑* ↑* ↑* ↔ — — ↑* ↑* ↑* ↑* ↑* 0°/180° 90°	F ↑* ↑* ↑* ↔ — — ↑* ↑* ↑* ↑* ↑* 0°/180° 90°
$4^2A'$	A — ↑ ↑ ↔ ↑ — ↑ ↑ ↑ ↑ ↑ 0°/180° 90°	B ↑ ↑ ↑ ↔ ↑ ↑ ↑ ↑ ↑ ↑ ↑ 0°/180° 90°	C ↑ ↑ ↑ ↔ — — ↑ ↑ ↑ ↑ ↑ 0°/180° 90°	D — ↑ ↑ ↔ ↑ — ↑ ↑ ↑ ↑ ↑ 0°/180° 90°	E — ↑ ↑ ↔ ↑ — ↑ ↑ ↑ ↑ ↑ 0°/180° 90°	F ↑* ↑* ↑* ↔ — — ↑* ↑* ↑* ↑* ↑* 0°/180° 90°
$4^2A''$	A — ↑ ↑ ↔ ↑ — ↑ ↑ ↑ ↑ ↑ 0°/180° 90°	B ↑ ↑ ↑ ↔ ↑ ↑ ↑ ↑ ↑ ↑ ↑ 0°/180° 90°	C ↑ ↑ ↑ ↔ — — ↑ ↑ ↑ ↑ ↑ 0°/180° 90°	D — ↑ ↑ ↔ — — ↑ ↑ ↑ ↑ ↑ 0°/180° 90°	E — ↑ ↑ ↔ — — ↑ ↑ ↑ ↑ ↑ 0°/180° 90°	F ↑* ↑* ↑* ↔ — — ↑* ↑* ↑* ↑* ↑* 0°/180° 90°

Evolution of the states in terms of configurations

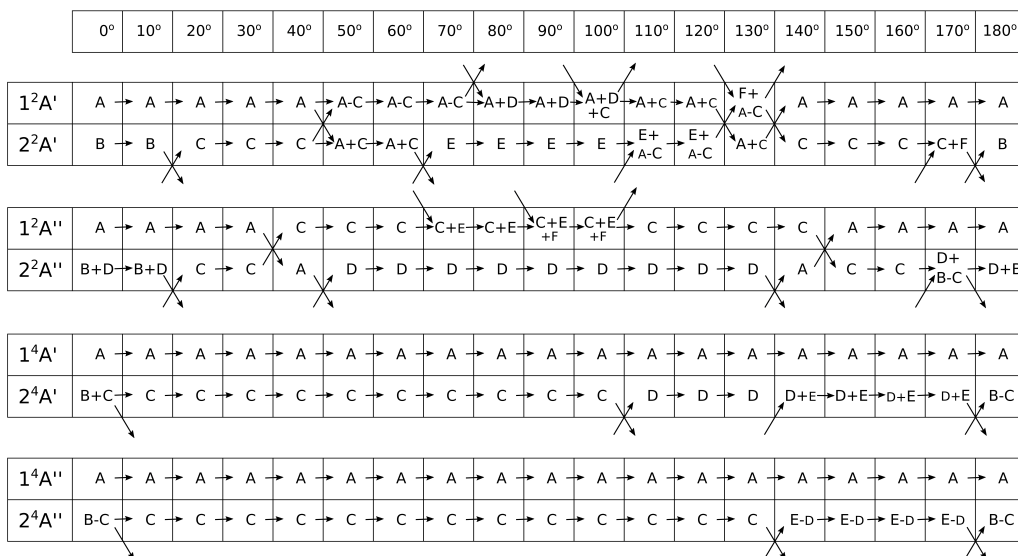


FIG. S7. MO diagram of the NO +O channel at fixed values of R and r together with details of the orbital occupancies. This Figure complements Figure 3 in the main text. The most important configurations with $>10\%$ contribution to the CASSCF wave function for each state are given in the middle panel of the figure. *Caption continued on next page.*

FIG. S7. *Continued*: Configurations where three single occupancies in orbitals couple to an overall doublet state are not distinguished further and so coupled orbitals indicated by an asterisk. Two configurations involve partially unoccupied bonding orbitals of the π_3 -systems (orbitals shown in Figure S8). In these extended MO diagrams, the additional orbitals are given in gray colour. The bottom panel reports which of the configurations contribute to the states for a given bending angle θ according to the CI coefficients from the CASSCF wave function (labels A to F). Smaller font indicates less contribution from a certain configuration. Arrows indicate the evolution of a configuration contribution to a state. I. e., crossing arrows indicate a change of configuration of a state, normally resulting in a configuration coupling and an avoided crossing of two states. States ${}^2A'$ and ${}^2A''$ are characterized by strong changes in contributing configurations along the path which is at the origin of the complexity of the shape of the PESs. Contrary to that, the ${}^4A'$ state only contains one configuration along the path which explains its rather simple topology.

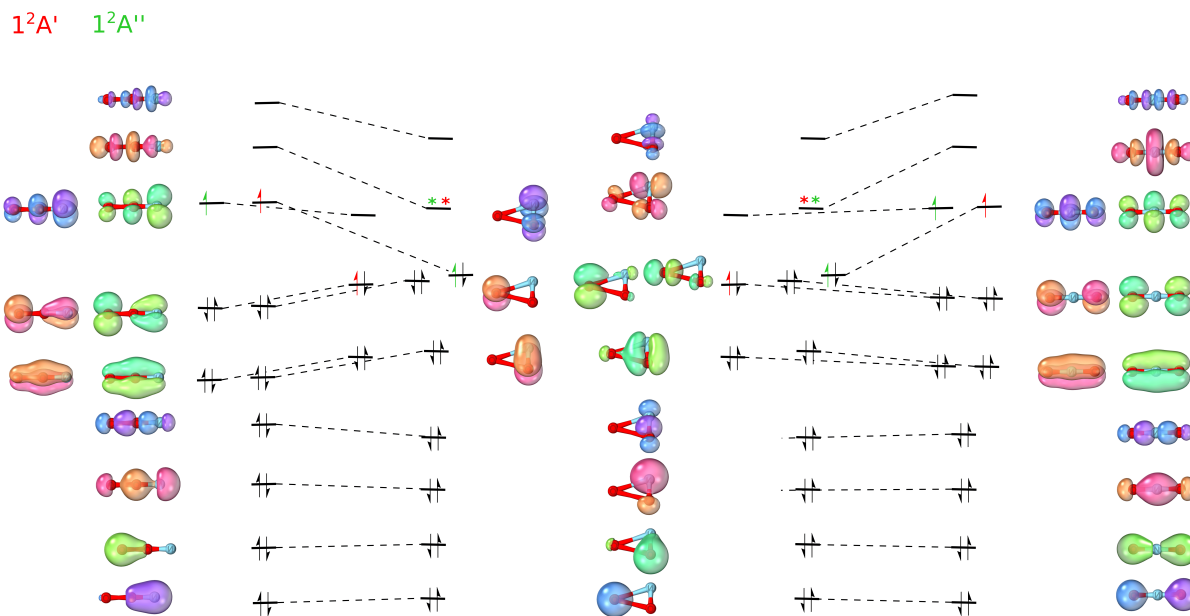


FIG. S8. MO diagram of NO₂ for the doublet ground state for the two linear configurations (left OON, right ONO) and for $\theta = 90$ (middle). The full valence orbital basis is shown. The dominant configurations at selected angles are depicted for the lowest ${}^2A'$ and ${}^2A''$ states. Black arrows for occupancies in both states, red for ${}^2A'$ and green for ${}^2A''$. Asterisks for significant additional occupancies due to strong correlation.

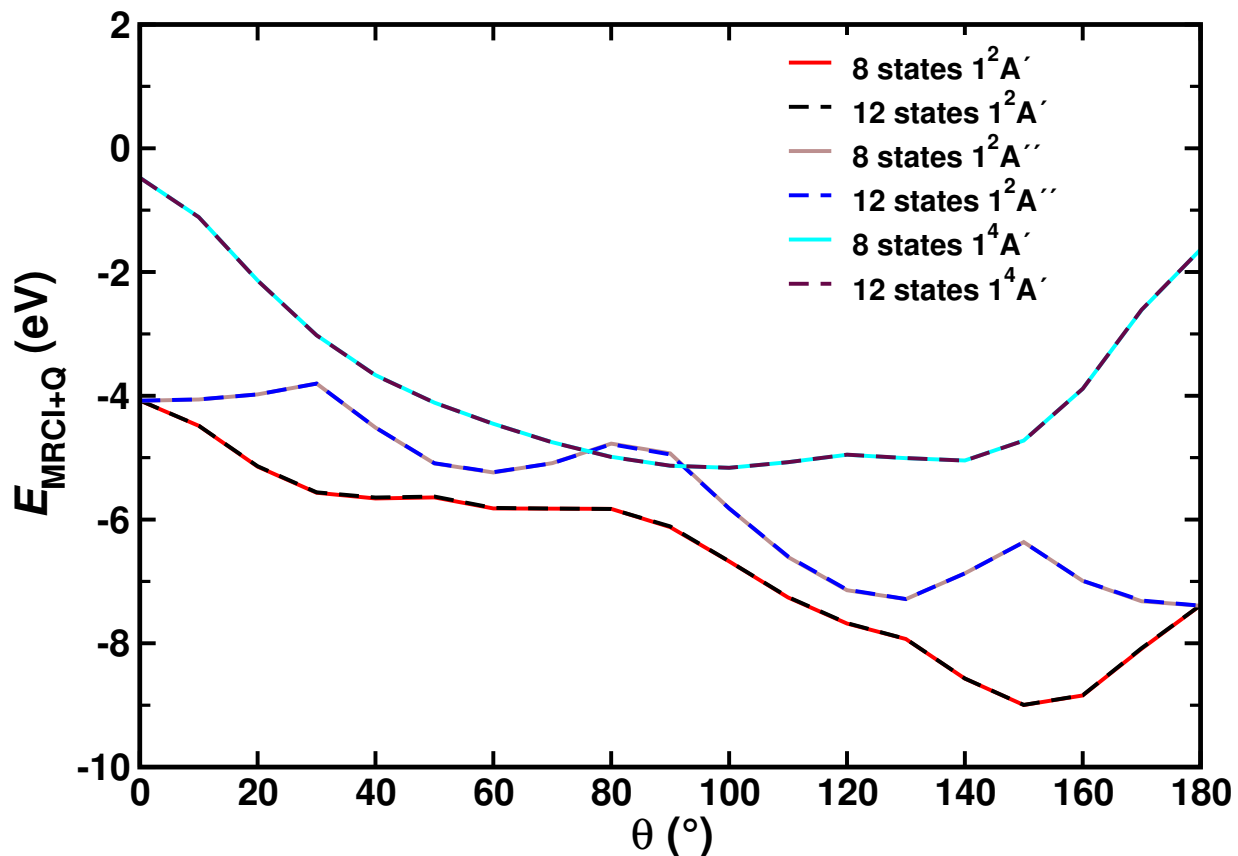


FIG. S9. The MRCI+Q energies for the 3 lowest states along the bending coordinate from an 8- and 12-state active space, see also Figure 3. The curves along the bending coordinate were determined for $R = 3.4 a_0$ and $r_{\text{NO}} = 2.183 a_0$ (equilibrium NO separation).

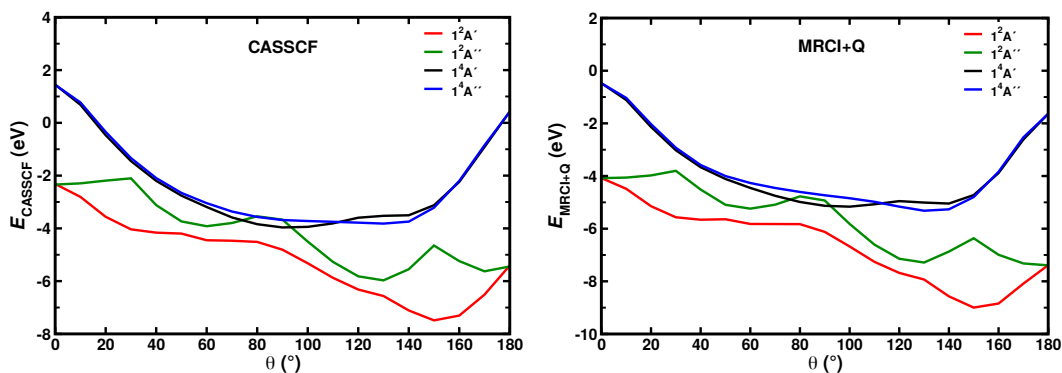


FIG. S10. Comparison of the CASSCF (left panel) and the MRCI+Q (right panel) energies for the 4 lowest states along the bending coordinate from an 8-state active space and including the full valence orbital space, see also Figures 3 and S9. The curves along the bending coordinate were determined for $R = 3.4 a_0$ and $r_{\text{NO}} = 2.183 a_0$ (equilibrium NO separation).

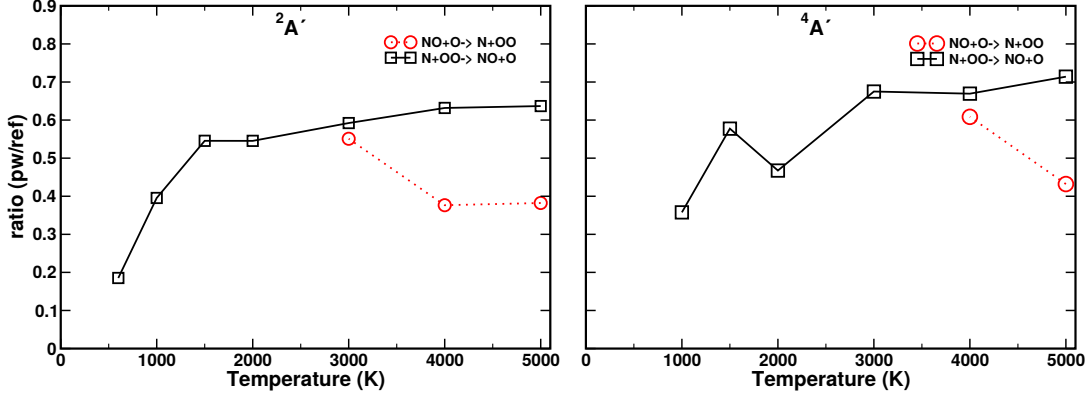


FIG. S11. Ratio between the present QCT and previously calculated ICVT³ thermal rates as a function of temperature. For the $^2A'$ (left) and $^4A'$ (right) using Gaussian binning for the forward ($N(^4S) + O_2(X^3\Sigma_g^-) \rightarrow O(^3P) + NO(X^2\Pi)$, solid line) and reverse ($O(^3P) + NO(X^2\Pi) \rightarrow N(^4S) + O_2(X^3\Sigma_g^-)$, dotted line) reaction.

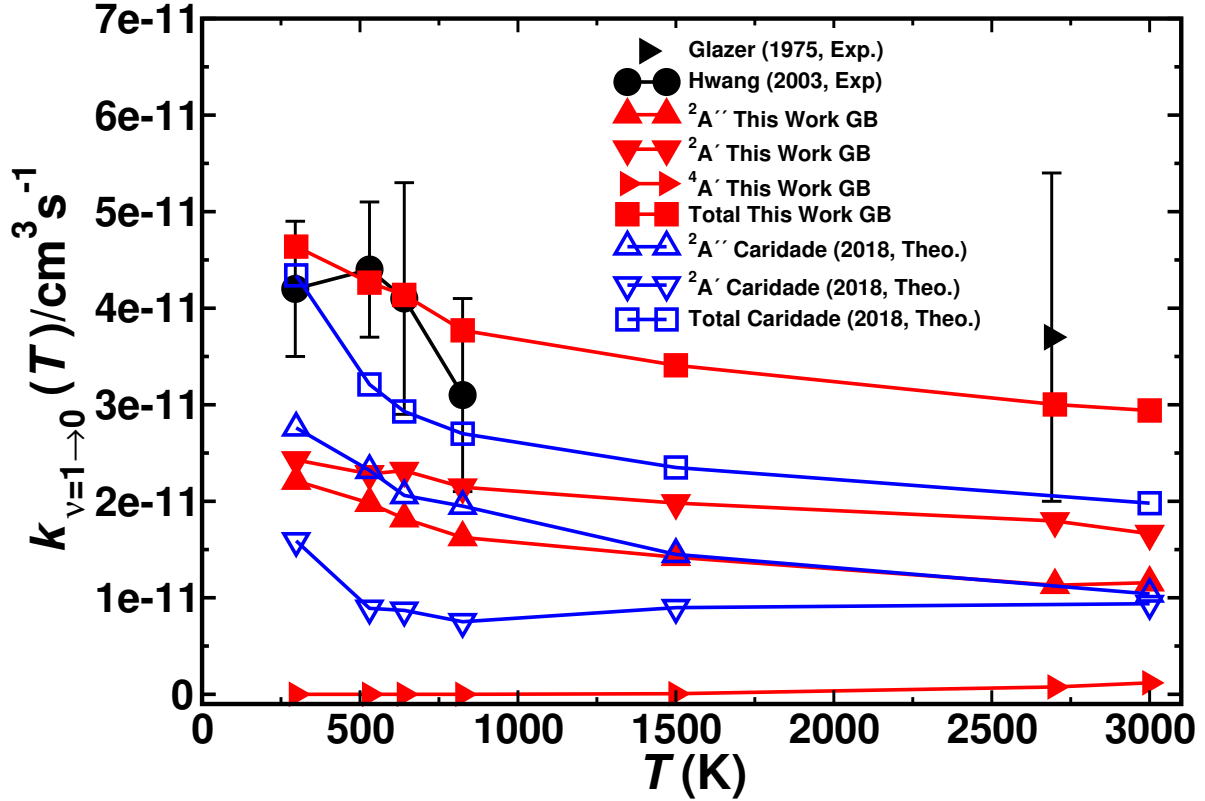


FIG. S12. Vibrational relaxation rates for $O+NO(\nu = 1) \rightarrow O+NO(\nu' = 0)$ computed on $^2A'$ (triangle down), $^2A''$ (triangle up) and $^4A'$ (triangle right) PESs. Results from this work are shown as filled symbols while from Ref.⁴ are shown as open symbols. The black filled symbols with error bars show the experimental results.

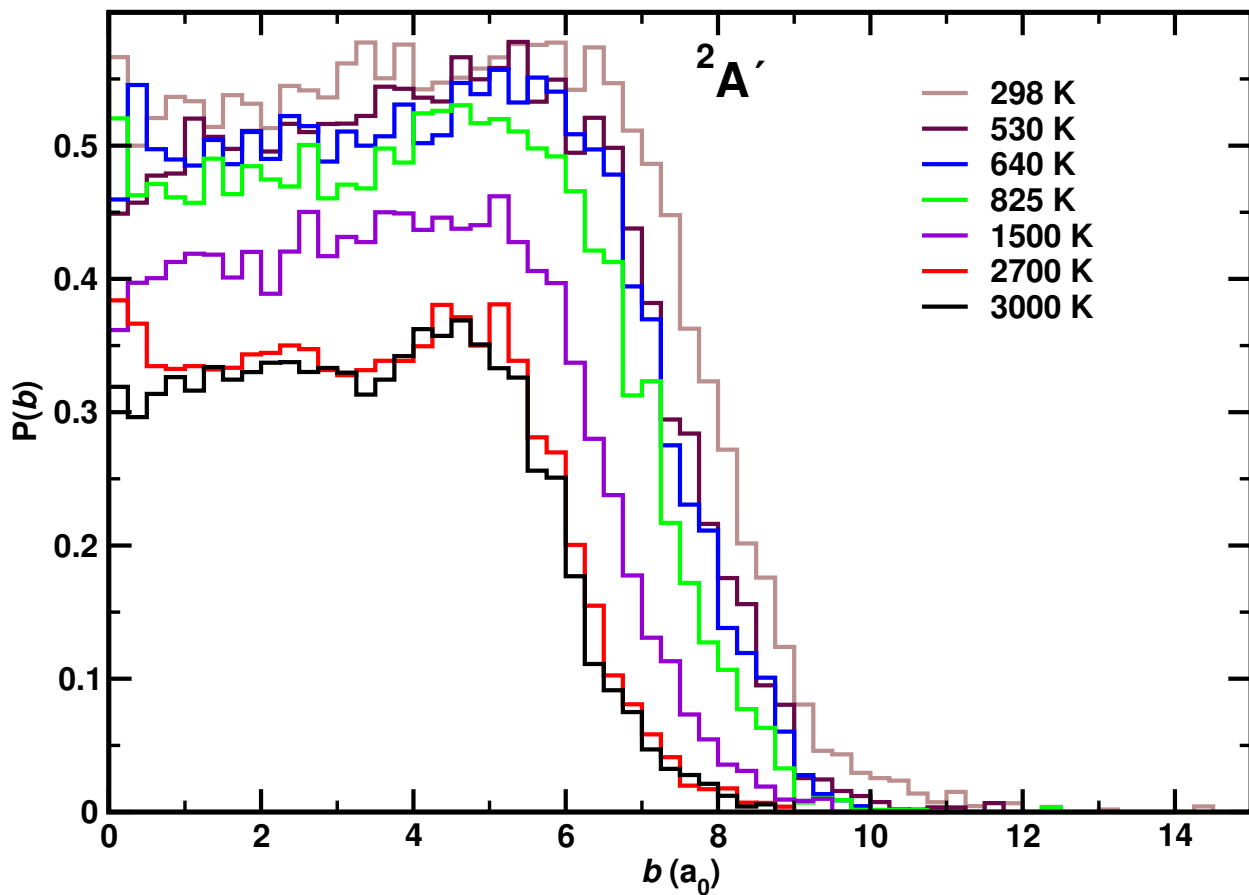


FIG. S13. Opacity function (probability of vibrational relaxation as a function of impact parameter) for the relaxing trajectories ($O + NO(\nu = 1) \rightarrow O + NO(\nu = 0)$), with or without oxygen atom exchange on the $^2A'$ PES at different temperatures. With increasing T the probability decreases and b_{\max} - the value for which vibrational relaxation still occurs - shifts to smaller values of b . The opacity function $P(b)$ indicates that at 300 K ~ 50 % of all trajectories starting in $O + NO(\nu = 1)$ relax to $O + NO(\nu = 0)$ for small values of b whereas at 3000 K only 30 % relax.

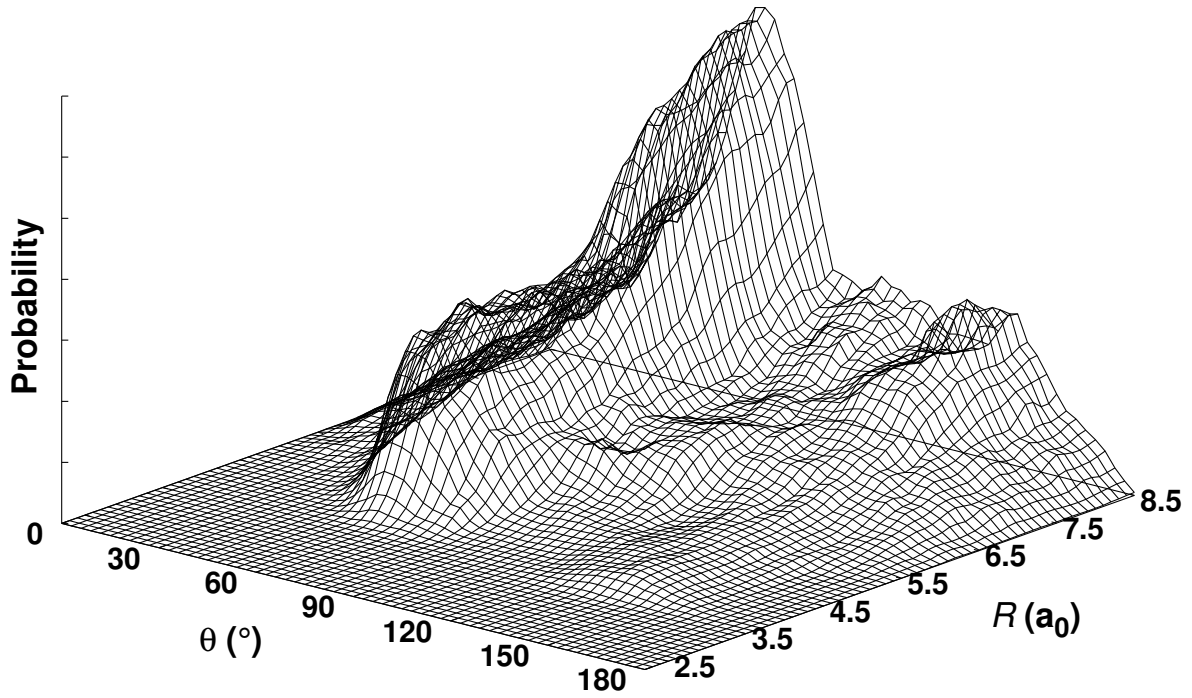


FIG. S14. Distribution of the vibrationally nonrelaxing trajectories in (R, θ) , i.e. $\text{O} + \text{NO}(\nu = 1) \rightarrow \text{O} + \text{NO}(\nu \neq 0)$, with or without oxygen atom exchange and $\text{N} + \text{O}_2$. The distance R is the oxygen atom-to-NO(center of mass) distance. Probability densities are calculated for all nonrelaxing trajectories and only up to the time satisfying the criterion that the sum of the three inter-nuclear distances is less than $9.5 a_0$.

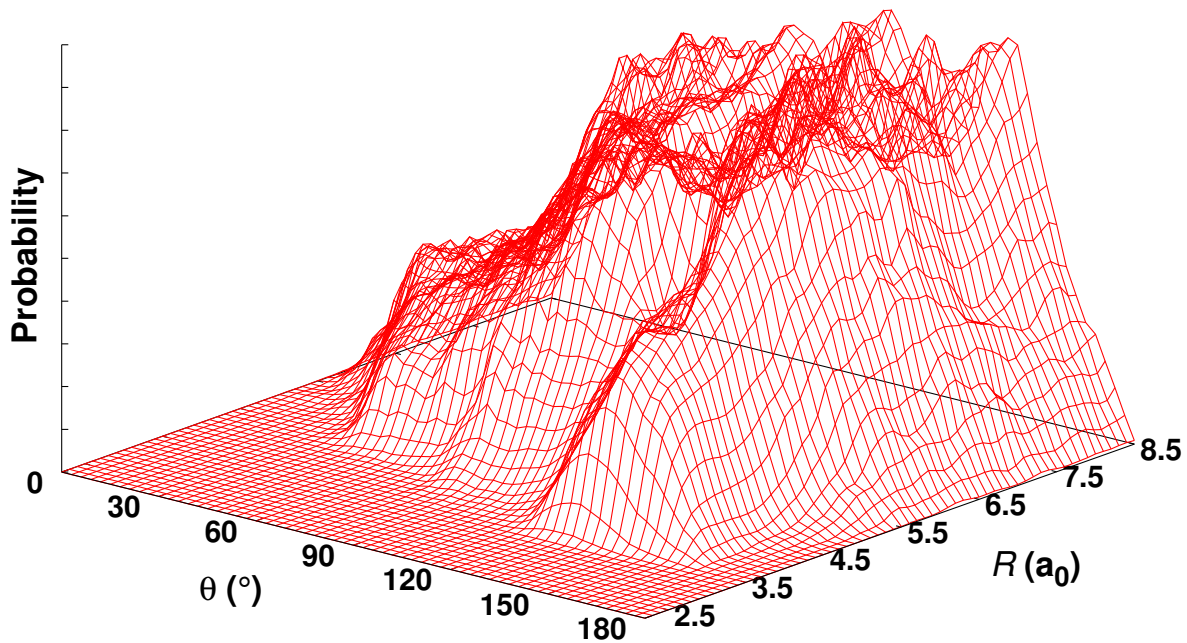


FIG. S15. Distribution of the vibrationally relaxing trajectories in (R, θ) , i.e. $\text{O} + \text{NO}(\nu = 1) \rightarrow \text{O} + \text{NO}(\nu = 0)$, with or without oxygen atom exchange. The distance R is the oxygen atom-to-NO(center of mass) distance. Probability densities are calculated for all relaxing trajectories and only up to the time satisfying the criterion that the sum of the three inter-nuclear distances is less than $9.5 a_0$.

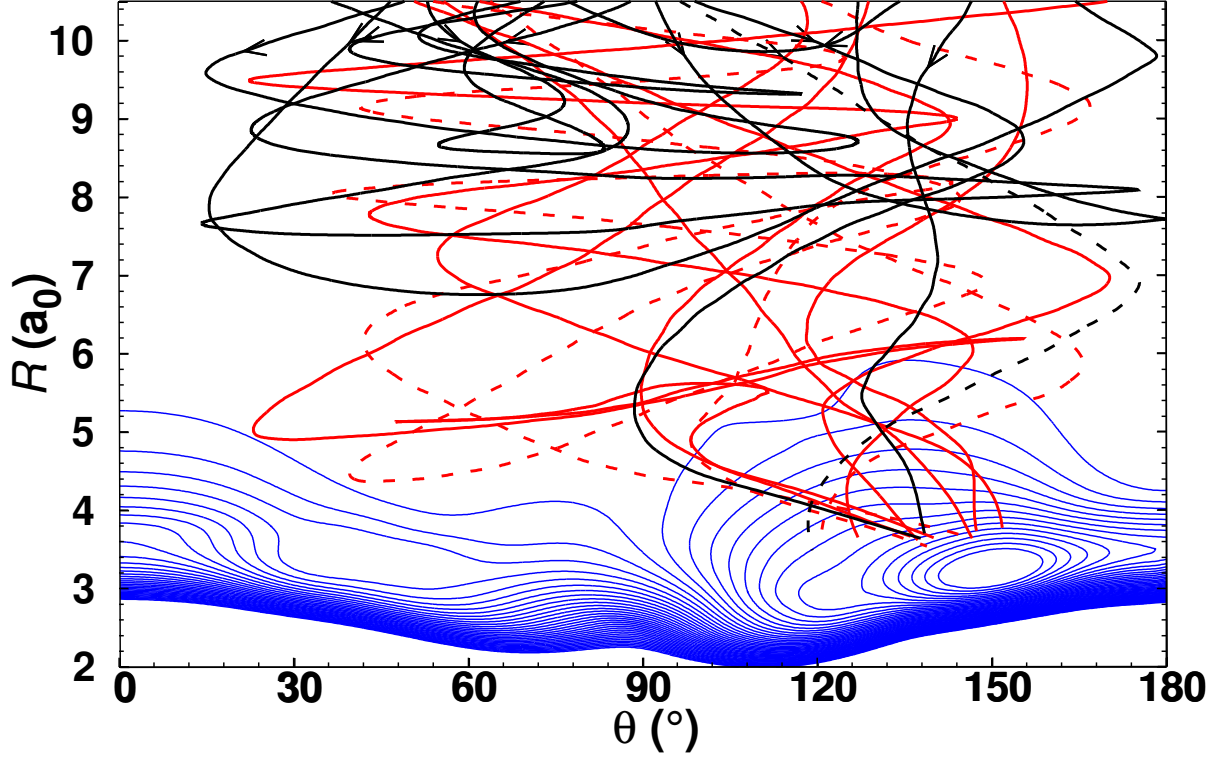


FIG. S16. Projection of vibrationaly relaxing (red) and nonrelaxing (black) O+NO collision trajectories onto the $^2A'$ PES (blue isocontours) as a function of (R, θ) . For each (R, θ) combination the energy of the structure with lowest energy for $r \in [2.03, 2.39]$ (covers the classical turning points of the $v_{\text{NO}} = 1$ vibration, which are at $r_{\text{min}} = 2.046 a_0$ and $r_{\text{max}} = 2.370 a_0$) is used. Ten random trajectories are shown for each of the cases. Trajectories are shown only up to the time satisfying the geometrical criterion that the sum of the three inter-nuclear distances is less than $9.5 a_0$. Reactive (oxygen exchange or O_2 formation) trajectories are shown as dashed lines.

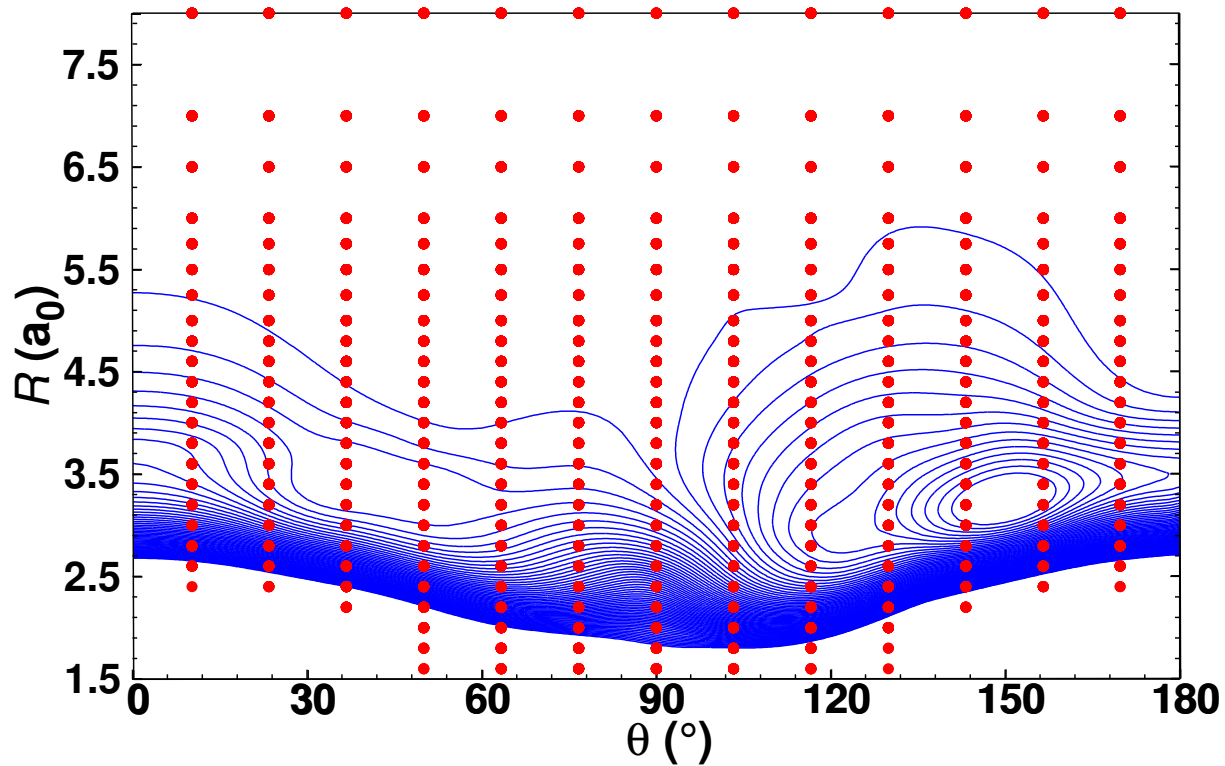


FIG. S17. Contour diagram of the relaxed PES (as a function of R , θ and $r = 2.03 - 2.39 a_0$) of the $^2A'$ PES for the O+NO channel. The *ab initio* grid points used in constructing the RKHS are shown as red filled circles at which MRCI+Q calculations were carried out.